Scientific paper

A Cohesive Interface Model for the Pullout of Inclined Steel Fibers in Cementitious Matrixes

Alessandro P. Fantilli[1] and Paolo Vallini[2]

Received 5 April 2007, accepted 15 May 2007

Abstract

The nonlinear behavior of fractured quasi-brittle materials is conventionally modeled with a fictitious crack model, which relates stresses on the crack surfaces to the corresponding crack widths. Its definition for fiber reinforced concrete is only possible by introducing a cohesive model for the matrix, and by modeling the pullout of randomly oriented fibers. To this aim, a new cohesive interface model, able to predict effectively the pullout response of inclined fiber, is presented in this paper. Based on the nonlinear behavior of steel fibers and cementitious matrixes, the proposed approach also takes into account the bond-slip relationship between the materials. By means of an iterative procedure, numerical results similar to experimental data can be obtained. In particular, maximum pullout forces at given inclination angles, as well as the complete pullout load vs. displacement diagrams, can be correctly predicted. Moreover, according to test results, the proposed approach shows, from the first pullout stage, the dependence of the response both on crushing of cementitious matrix and on yield strength of steel fibers.

1. Introduction

Fracture energy of Fiber Reinforced Cementitious Composites (FRC) can be higher than that released by traditional cement-based concretes. Practically, in the cohesive relationship, at a given crack width, higher tensile stresses can be detected on the crack surfaces of FRC, because of the bridging effect produced by fibers. To better define this phenomenon, the pullout response of a single fiber in a cementitious matrix needs to be investigated (Hillerborg, 1980).

Pullout involves fibers inclined with respect to crack surfaces, as they are randomly positioned within the matrix. This has been investigated both theoretically and experimentally (see e.g., Shah *et al*., 2004). In a huge number of tests, fibers made of different materials and shapes have been pulled out from cement-based or plastic specimens. For the sake of simplicity, only pullout of straight steel fibers in a cementitious matrix is considered in the present paper.

In the first tests by Naaman and Shah (1976), the maximum pullout load of inclined fibers appeared higher than that measured in specimens with aligned fibers (fibers direction orthogonal to crack surfaces). Moreover, if the pullout diagram (that is, load P vs. displacement w) of an aligned fiber ends approximately with zero loads, in case of inclined fibers a significant load persists up to the complete slippage. In other words, due to the nonlinear behavior of materials, the area under a P - w curve, usually called pullout work, generally increases with fiber inclination. For these reasons, according to the results of Leung and Shapiro (1999), in specimens having the same cementitious matrix, the yield strength of steel fibers plays a fundamental role on the crack-bridging efficiency. In fact, at the same inclination angle, both the maximum load and the pullout work seem to increase with the yield strength of steel fibers (Leung and Shapiro, 1999).

It must be remarked that bond properties and yield strengths are strictly connected to fiber production (e.g. hot rolled or cold drawn, see CEB, 1991). Thus, to model the pullout of inclined fibers, the bond-slip mechanism between fiber and matrix cannot be neglected. This is also confirmed by the pullout tests conducted on unbonded fibers (Kohno and Mihashi, 2005). Although their pullout work is nearly equal to zero when fibers are orthogonal to crack surfaces, significant values of the maximum load and of the pullout work can be equally observed in the case of inclined fibers. Depending on the way this mechanism is taken into consideration, the models reported in the current literature can be classified into different groups (Shah and Ouyang, 1991).

Classical approaches assume that the condition of perfect bond persists till either stress or energy criterion is exceeded on the interface of fiber and matrix. In models founded on stress criterion, debonding begins and slip between fiber and matrix takes place after the maximum admissible value of bond stress is reached (Stang *et al*., 1990). Constant bond stresses are assumed to be present in the debonded zone (pure frictional model), while in the remaining part of the fiber the condition of perfect bond (zero slips) is assumed. Several pullout models have been founded on this criterion, like the analytical solution proposed by Morton and Groves (1974), and the most recent numerical approach intro-

[1]Assistant Professor, Department of Structural and Geotechnical Engineering, Politecnico di Torino, Italy.
E-mail: alessandro.fantilli@polito.it
[2]Professor, Department of Structural and Geotechnical Engineering, Politecnico di Torino, Italy.

duced by Katz and Li (1995). In addition to the debonding phenomenon, the last model is able to take into account the stiffness contribution of the fiber portion which protrudes from the matrix (assumed to be in the linear elastic regime), while the embedded part of fiber interacts with the matrix similar to a beam on elastic foundation (Leung and Li, 1992).

Very few models have been based on the energy criterion. In this case, only when the energy release rate of debonding reaches its critical value, does slip between materials begin (Shah and Ouyang, 1991). Because of difficulties in measuring the critical interface debonding energy, these approaches cannot be applied to real cases, with the exception of the model proposed by Brandt (1985) to define the optimal inclination angle.

Besides stress and energy criteria, the pullout of inclined fibers can be investigated by means of the so-called cohesive interface models, in which bond stresses are only due to slip between steel and cement-based matrix (Shah and Ouyang, 1991). Such models, as well as the tension stiffening investigation of reinforced concrete structures, consist of the classical equilibrium and compatibility equations (Fantilli *et al*., 1998). Cohesive interface models are seldom used in the case of fiber pullout, because bond properties of fiber and matrix cannot be generalized, but have to be measured in each single case (Shah and Ouyang, 1991). Moreover, the mathematical solution of the problem does not generally carry out analytical formulae, and therefore numerical iterative procedures are needed. This has been done by Fantilli and Vallini (2003a) to model the complete pull-out response of aligned steel fibers in cementitious matrixes. Such a model, based on the definition of a suitable bond-slip relationship (Fantilli and Vallini, 2003b), is here extended to the analysis of fibers inclined with respect to crack surfaces.

2. Equilibrium and compatibility equations of a cohesive interface model

The bridging action of a fiber, initially inclined of α respect to the crack surfaces of a cementitious matrix, is shown in **Fig. 1**. The crack width $2w$ is produced by a horizontal displacement (w = pullout displacement) imposed to the whole composite (**Fig. 1b**). The final position of the fiber is illustrated in **Fig. 1c**, where, due to symmetry, only half fiber is shown.

When $w > 0$, the points named A, A' and A", which coincide for $w = 0$, will be separated as a consequence of a slip s between fiber and matrix, and of matrix spalling failure that affects the length d (measured on the original position of the fiber). According to Leung and Li (1992), the pullout load P, which has to be applied in order to produce the displacement w, can be computed by splitting the fiber into two parts (**Fig. 1c**): the block delimited by the points A" and B" (named block A"-B"), which protrudes from the matrix, and the block delimited by the points B" and C'(named block B"-C'), which is embedded in the matrix. C and C' are the position of fiber's end before and after the application of w, respectively.

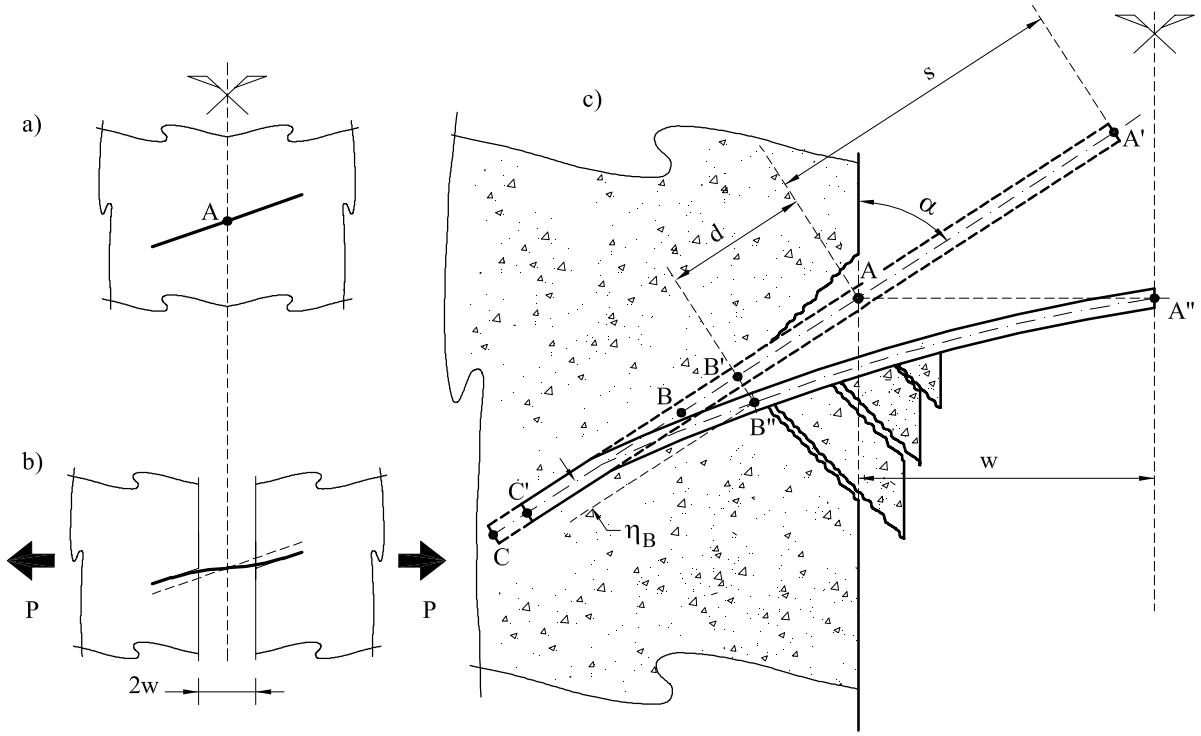

Fig. 1 Pullout of an inclined fiber: a) undeformed state ($w = 0$); b) deformed state ($w \neq 0$); c) position of the fiber at a given displacement w (or load P).

2.1 The block A"-B"

The initial position of the fiber, defined in **Fig. 1c** by the points A and B and by the angle α, changes in consequence of the displacement w. The new position, defined by the point A" and B" in **Fig. 2**, is univocally defined by the kinematical variables α, d, and w, and by the effects of matrix deformation (i.e. the rotation θ_B and the displacement η_B of the point B"). Therefore, the real length l_0 of the block A"-B" and the complete rotation δ of the fiber can be respectively computed with the following equations:

$$l_0 = \sqrt{(d\cos\alpha + \eta_B \sin\alpha)^2 + (d\sin\alpha - \eta_B \cos\alpha + w)^2} \quad (1)$$

$$\delta = \frac{\pi}{2} - \alpha - tg^{-1}\left(\frac{d\cos\alpha + \eta_B \sin\alpha}{d\sin\alpha - \eta_B \cos\alpha + w}\right) \quad (2)$$

where $\pi = 3.1426$. The angle δ can be considered as the sum of three different rotations:

$$\delta = \theta_B + \theta_i + \theta_t \quad (3)$$

where θ_t = rotation produced by shear actions; θ_i = rotation produced by bending moment. Both elastic and plastic components (named θ_e and θ_p) have to be included in the last rotation:

$$\theta_i = \theta_e + \theta_p \quad (4)$$

When all these contributions are known, the apparent length l_t of the block A"-B" (**Fig. 2**) and the slip s are obtained as follows:

$$l_t = l_0 \cos\theta_i + \Delta z \quad (5)$$

$$s = l_t - d \quad (6)$$

The apparent length reduction Δz, which appears in the Eq. (5), is a function of the deflection $\eta_i(z)$ of the fiber. If a sinusoidal function is assumed for $\eta_i(z)$, the apparent shortening has the following form:

$$\Delta z = \frac{1}{2}\int_{l_z}\left(\frac{\partial \eta_i}{\partial z}\right)^2 dz = \frac{\pi^2}{16}\frac{l_y^{\,2}}{l_z}$$

$$\text{if} \quad \eta_i = l_y\left(1 - \cos\frac{\pi z}{2 l_z}\right) \quad (7)$$

where $l_z = l_0 \cos\theta_i = z$ component of l_0 (**Fig. 2**); $l_y = l_0 \sin\theta_i$ = maximum deflection of the fiber (y component of l_0).

The static conditions of the block A"-B" is depicted in **Fig. 3a**. Due to symmetry, the bending moment M_A=0, while both shear and normal forces, defined respectively in the y and z directions, are constant in each cross-section of the fiber (T_A=T_B and N_A=N_B). Therefore, by considering second order effects, the bending moment at the point B" results:

$$M_B = T_A l_0 \cos\theta_i - N_A l_0 \sin\theta_i \quad (8)$$

Under the hypothesis of linear elastic behavior, the rotations θ_t and θ_e of the fiber can be written as functions of T_B and M_B, respectively:

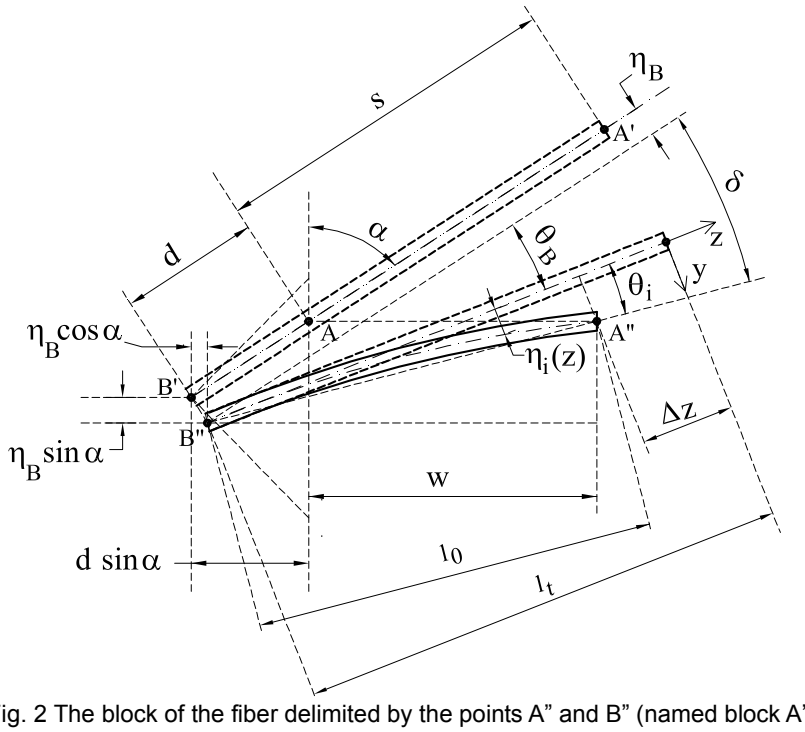

Fig. 2 The block of the fiber delimited by the points A" and B" (named block A"-B").

$$\theta_t = T_B \frac{f_t}{G_f A_f} \tag{9}$$

$$\theta_e = M_B \frac{4 l_z}{\pi^2 E_f J_f} \tag{10}$$

where, f_t = dimensionless shear constant (for a circular cross-section $f_t = 32/27$); G_f = shear modulus of the fiber; E_f = Young's modulus of the fiber; A_f = area of the fiber cross-section; J_f = moment of inertia of the fiber cross-section.

In the block A"-B" of length $l_z = n\,\Phi$ (Φ = diameter of the fiber cross-section; n = integer number), it can be of practical interest to evaluate the ratio q_T between shear and flexural rotations:

$$q_T = \frac{\theta_t}{\theta_e} = 0.402 \frac{\Phi}{n} \tag{11}$$

From Eq.(11) it is possible to observe the necessity of taking into account the shear contribution to rotation in case of narrow crack widths (that is $l_z < 10\,\Phi$).

2.2 The block B"-C'

For the embedded part of the fiber, modeled as a beam on elastic foundation (Leung and Li, 1992), it is possible to introduce a relationship between the kinematical variables (θ_B and η_B) and the static actions (T_B and M_B):

$$\begin{Bmatrix} \eta_B \\ \theta_B \end{Bmatrix} = \begin{bmatrix} d_{11} & d_{12} \\ d_{21} & d_{22} \end{bmatrix} \begin{Bmatrix} T_B \\ M_B \end{Bmatrix} \tag{12}$$

where the coefficients d_{ij} of the deformability matrix (that is, the inverse of the stiffness matrix) have to be evaluated as functions of the matrix foundation stiffness K. If the Young's modulus E_m and the Poisson's ratio ν_m of the matrix are known, K is given by (see **Fig. 3c** and Appendix 2):

$$K = \frac{E_m \left(1 - \nu_m^2\right)}{2.651} \tag{13}$$

According to the classical books on foundations (Hetenyi, 1946; Bowles, 1988), the differential equation for the deflection curve of a beam supported on an elastic foundation is based on the factor β, whose inverse is usually called characteristic length. In the present case, it connects the flexural stiffness of the fiber ($E_f J_f$) and the matrix foundation stiffness previously computed:

$$\beta = \sqrt[4]{\frac{K}{4 E_f J_f}} = \sqrt[4]{\frac{6.04\, E_m \left(1 - \nu_m^2\right)}{E_f \pi \Phi^4}} \tag{14}$$

If the length of the considered block $l_{BC} = l_i - d\text{-}s \geq \pi/\beta$ (**Fig. 3b**), the embedded part of the fiber can be considered as a long beam and therefore the coefficients d_{ij} of Eq. (12) are those of a semi-infinite beam with free end (Hetenyi, 1946; Bowles, 1988):

$$d_{11} = \frac{1}{2\beta^3 E_f J_f} \quad d_{12} = d_{21} = \frac{1}{2\beta^2 E_f J_f} \quad d_{22} = \frac{1}{\beta E_f J_f} \tag{15}$$

On the contrary, if $l_{BC} \leq 0.25\,\pi/\beta$, the supported part of the fiber can be considered absolutely rigid (like a short beam), thus d_{ij} can be determined by simple static considerations:

$$d_{11} = \frac{4}{K l_{BC}} \quad d_{12} = d_{21} = \frac{6}{K l_{BC}^2} \quad d_{22} = \frac{12}{K l_{BC}^3} \tag{16}$$

When the block B"-C' is of medium length, $0.25\,\pi/\beta < l_{BC} \leq \pi/\beta$, the coefficients d_{ij} of Eq. (12) are computed by means of a linear interpolation of Eq. (15) and Eq. (16).

The axial load N_B in the cross-section B" of the fiber can be considered as a function of the bond load N_{bs} and of the actions T_B and M_B:

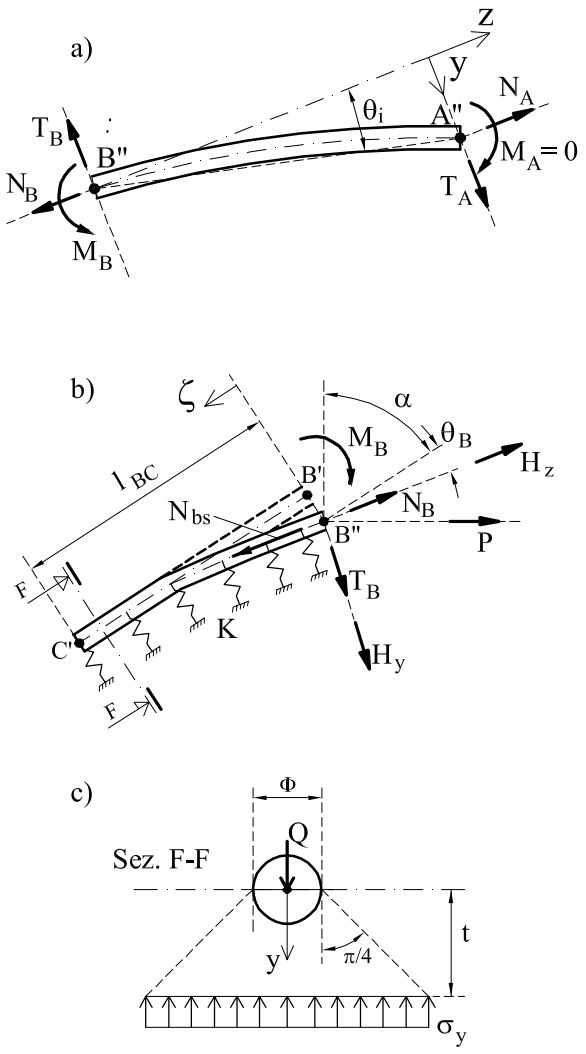

Fig. 3 Free body diagrams of the inclined fiber: a) actions in the block A"-B"; b) actions in the block B"-C'; c) stress-diffusion in the section F-F.

$$N_B = N_{bs} + K_M M_B + K_T T_B \tag{17}$$

where the coefficients K_T and K_M are computed with the hypotheses that the embedded part of the fiber lies on an elastic matrix foundation and by assuming a suitable friction coefficient γ between materials. If $l_{BC} \geq \pi/\beta$ (**Fig. 3b**), the coefficients K_T and K_M are respectively (Hetenyi, 1946; Bowles, 1988):

$$K_T = \frac{\gamma K}{T_B} \int_{l_{BC}} |y(T_B)| dz \cong 1.4\gamma \tag{18a}$$

$$K_M = \frac{\gamma K}{M_B} \int_{l_{BC}} |y(M_B)| dz \cong \frac{\gamma}{\Phi} \tag{18b}$$

In the case of short beam ($l_{BC} \leq 0.1\ \pi/\beta$) the previous coefficients can be written as:

$$K_T = \frac{\gamma K}{T_B} \int_{l_{BC}} |y(T_B)| dz \cong \frac{5}{3}\gamma \tag{19a}$$

$$K_M = \frac{\gamma K}{M_B} \int_{l_{BC}} |y(M_B)| dz \cong \frac{3\gamma}{l_{BC}} \tag{19b}$$

For medium lengths, $0.25\ \pi/\beta < l_{BC} \leq \pi/\beta$, the coefficients K_T and K_M are computed by means of a linear interpolation of Eqs. (18) and Eqs. (19).

Since the bond force N_{bs} is a function of the slip $s_{fm}(\zeta)$ between fiber and matrix within the block B"-C' (**Fig. 3b**), it can be obtained by solving the classical tension-stiffening problem, which consists of the following system of equilibrium and compatibility equations (Fantilli and Vallini, 2003a):

$$\begin{cases} \dfrac{ds_{fm}}{d\zeta} = -\varepsilon_f \\ N(\zeta) = A_f\, \sigma_f \\ \dfrac{d\sigma_f}{d\zeta} = -4\dfrac{\tau(\zeta)}{\Phi} \end{cases} \tag{20}$$

where ε_f = axial strain in the fiber; σ_f = axial stress in the fiber; and $\tau(\zeta)$ = bond stresses at fiber-matrix interface. To solve Eqs. (20), the boundary conditions [$N(\zeta=0) = N_{bs}$ and $N(\zeta = l_{BC}) = 0$] and a suitable bond-slip relationship $\tau(s)$ have to be introduced. In this way, all the possible bond mechanisms (e.g., slip softening or slip hardening) are taken into account in the computation of normal force N_{bs}. Thus, according to Shah and Ouyang (1991), the proposed approach can be classified in the family of cohesive interface models.

When N_{bs} is known, Eq. (17) can be inserted into Eq. (8) ($N_A = N_B$ and $T_A = T_B$), in order to obtain a new equation for the shear force T_B :

$$T_B = \frac{M_B\left(1 + K_M\, l_0 \sin\theta_i\right) + N_{bs}\, l_0 \sin\theta_i}{\left(l_0 \cos\theta_i - K_T\, l_0 \sin\theta_i\right)} \tag{21}$$

3. A possible solution of the problem

From the equations written in the previous section, the complete pullout diagrams (load P vs. displacement w) can be theoretically defined and compared with those measured experimentally. This is possible after defining the constitutive relationships of materials, their interaction [that is, $\tau(s)$ function], and by introducing a numerical procedure for the solution of the problem.

3.1 The bond-slip relationship and the friction coefficient between fiber and matrix

For smooth steel fibers in a cementitious matrix, the model proposed by Fantilli and Vallini (2003b) can be adopted. It consists of an improvement and an extension of the classical model proposed by Model Code 90 (CEB, 1991) for smooth steel reinforcing bars. In particular, both for bars and fibers, the post peak softening is introduced in conjunction with the size effect produced by fiber diameter on bond strength. The ascending branch and the post-peak stage of the proposed bond-slip relationship (**Fig. 4a**) are respectively defined by the following equations:

$$\tau = \tau_{\max}\left(\frac{s}{s_1}\right)^{0.5} \qquad \text{if } s \leq s_1 \tag{22a}$$

$$\tau = \tau_{fin} + \left(\tau_{\max} - \tau_{fin}\right) e^{k(s_1 - s)} \qquad \text{if } s > s_1 \tag{22b}$$

where τ_{max} = bond strength; s_1 = slip at bond strength; τ_{fin} = asymptotic value of bond stress; k = coefficient. These parameters are defined in **Fig. 4b** as a function of bond conditions, of the type of smooth bar (hot rolled or cold drawn), and of the compressive strength f_c of the matrix.

The maximum bond stress is here considered as a function of the fiber diameter according to the Bazant's size effect law (Bazant *et al*., 1995) for hot rolled bars and for cold drawn wires, respectively:

$$\tau_{\max} = \frac{1.572}{\sqrt{12.5 + \Phi}}\sqrt{f_c} \tag{23a}$$

$$\tau_{\max} = \left(\frac{1.572}{\sqrt{12.5 + \Phi}} - 0.2\right)\sqrt{f_c} \tag{23b}$$

where τ_{max} and f_c are measured in MPa, while Φ is measured in mm.

The bond-slip relationship previously defined cannot be used for all kind of fibers. Nevertheless, if a new τ-s has to be defined for other types of fiber (hooked, twisted, etc.), the procedure proposed in Fantilli and Vallini (2003b) can be adopted. In particular, after defining the shape of the relationship, the possible variation of its parameters should be measured, at different scales, by means of pullout tests on aligned fibers.

The cold or hot manufacturing of reinforcement steel produces not only different bond stresses between bars

a)

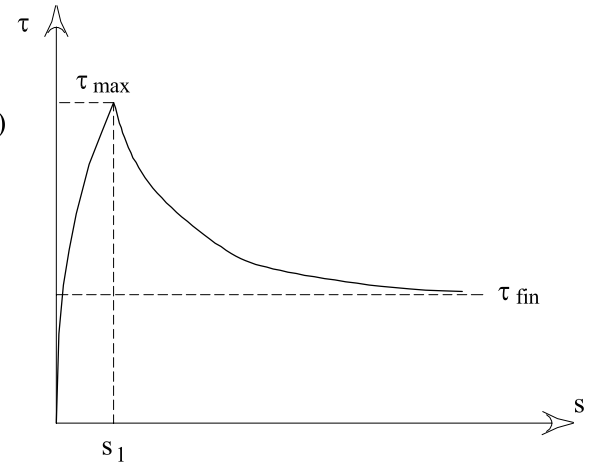

b)

	Cold drawn wires	Hot rolled bars
	Good Bond conditions	Good Bond conditions
s_1	0.01 mm	0.1 mm
k	2 / mm	2 / mm
τ_{fin}	$0.067\sqrt{f_c}$	$0.1\sqrt{f_c}$

Fig. 4 Bond properties of smooth steel fiber: a) the bond-slip relationship $\tau(s)$; b) parameters of $\tau(s)$ defined in the cases of cold drawn wires and hot rolled bars (Fantilli and Vallini, 2003b).

(or fibers) and matrixes, but also different friction coefficients γ. Since no experimental campaign has been devoted to evaluate all the possible values of such coefficient, it must be considered as a free parameter, which can vary within the range 0.1÷0.3 in case of steel fibers in cementitious matrixes.

3.2 The mechanical behavior of steel fibers

The pullout tests by Leung and Shapiro (1999) clearly show the importance of yield strength f_y of inclined steel fibers in a cementitious matrix. For this reason, it is necessary to take into account the nonlinear response of fibers, which is here included in the bilinear stress-strain σ_f-ε_f relationship depicted in **Fig. 5a**. In this diagram, the linear elastic branch is univocally defined by the Young's modulus E_f, whereas the non linear stage, assumed to be perfectly plastic, is only defined by the yield strength f_y.

Yielding of an inclined steel fiber is generally reached around point B" (**Fig. 2**), where fiber cross-section is contemporarily subjected to normal, shear and bending actions (N_B, T_B and M_B, respectively). At this stage, the plastic rotation θ_p [Eq. (4)], which is zero during the elastic stage, can be increased indefinitely. The definitions of the yield surface of a fiber, having a circular cross-section and subjected to N_B, T_B and M_B, is therefore of primary importance. For instance, this is possible by means of Hodge's approach (Chen and Han, 1988). However, in the case of a circular cross-section made of an elastic-plastic material (**Fig. 5a**), it provides a yielding surface which can be adequately modelled by the following ellipsoidal equation:

$$\lambda = \left(\frac{M_B}{M_0}\right)^2 + \left(\frac{N_B}{N_0}\right)^2 + \left(\frac{T_B}{T_0}\right)^2 \tag{24}$$

where M_0, T_0 and N_0 are, respectively, the limiting yield values of bending moment, shear and normal forces of a circular cross-section (Chen and Han, 1988). If the values of N_B, T_B and M_B give $\lambda > 1$, yield conditions are violated, thus there must be an increase of θ_p until Eq. (24) gives $\lambda = 1$.

3.3 The mechanical behavior of damaged matrix

Undamaged matrix generally behaves linearly. When failure conditions are reached, damage occurs and pieces of matrix are progressively broken away from the fiber. As **Fig. 1c** shows, the damaged zone progressively increases its length d with the increase of w. To be more precise, the position of point B" should be closer to the point C', if the resultant of the applied loads exceed matrix strength. Referring to the beam on elastic foundation depicted in **Fig. 3b**, the normal force H_y transferred by the fiber to the matrix is (Hetenyi, 1946; Bowles, 1988):

$$H_y = K\int_0^{8/\beta} |y(M_B)|dz + K\int_0^{4/\beta} |y(T_B)|dz == \frac{\pi\beta}{4}M_B + \frac{\pi}{2}T_B \tag{25}$$

The resultant of applied loads can be obtained by combining H_y and the friction forces H_z of Eq. (17), which are supposed to be applied at point B" (**Fig. 3b**):

$$H_z = K_M M_B + K_T T_B \tag{26}$$

If the linear Mohr-Coulomb failure criterion is assumed for the cementitious matrix (**Fig. 5b**), the fractured cone surface has its axis parallel to y under pure compression (**Fig. 5c**); whereas, in pure tension, the axis is parallel to z (**Fig. 5d**). In these cases, matrix resistances are given respectively by:

$$R_y = \frac{\pi(d\sin\alpha)^2}{2} f_c \tag{27a}$$

$$R_z = \pi(d\sin\alpha\, tg\psi)^2 f_{ct} \tag{27b}$$

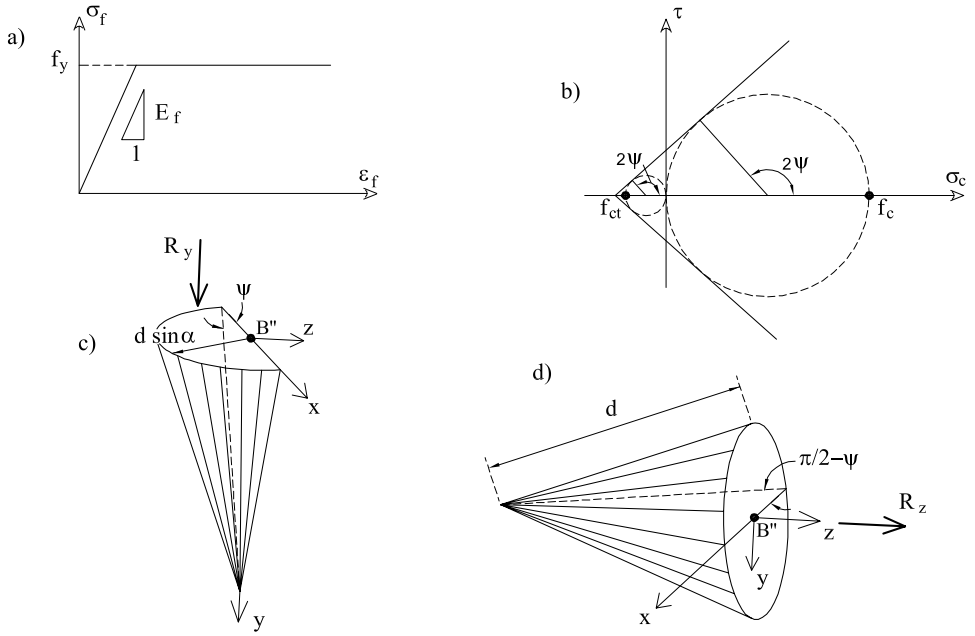

Fig. 5 Mechanical behavior of materials: a) stress-strain relationship for steel fibers; b) failure criterion adopted for the cementitious matrix; c) failure surface of matrix under compression; d) failure surface in tension.

where f_{ct} = tensile strength of the matrix; ψ = angle defined by principal directions in the linear Mohr-Coulomb failure criterion (**Fig. 5b**). If a cementitious matrix is considered, then $f_{ct} = 0.1\, f_c$ and $\psi \cong 72°$.

In the case of combined stresses, the following failure surface can be assumed for the matrix:

$$\lambda = \frac{H_z}{R_z} + \frac{H_y}{R_y} \tag{28}$$

Equation (28) needs to be introduced because of the biaxial state of stress that affects the cohesive response of the matrix. In particular, the post peak response in the y direction is affected, and reduced, by the stresses and the damage produced in the z direction, and vice versa. If the values of H_z and H_y give $\lambda > 1$, the failure condition of the matrix is violated, thus d must be increased until Eq. (28) provides $\lambda \le 1$.

3.4 A numerical procedure to obtain the pullout diagram

Due to nonlinear behavior of materials and to their mutual interaction (i.e. the bond-slip relationship), the P-w diagram of a pullout test can be numerically obtained by solving the equations previously introduced, with the following iterative procedure:

(1) Select a pullout displacement w;
(2) Assume trial values for the plastic rotation θ_p and for the damaged length d (for instance those computed for the lower values of w);
(3) Assume trial values for θ_B, η_B and for the coefficients d_{ij} (for instance those computed for the lower values of w);
(4) Compute the actions M_B and T_B through Eq. (12);
(5) Compute the final position of the fiber by evaluating l_0 [Eq.(1)], δ [Eq.(2)], θ_t [Eq.(9)], θ_i [Eq.(3)], Δz [Eq.(7)], l_t [Eq.(5)], s [Eq.(6)] and the embedded length $l_{BC} = l_i - d - s$;
(6) Compute the bond force N_{bs} by solving the tension-stiffening problem [Eqs.(20)];
(7) Evaluate the coefficients d_{ij} [Eqs. (15)-(16)] and K_M, K_T [Eqs. (18)-(19)] in accordance with the last value of l_{BC};
(8) Compute new values for M_B and T_B with Eq. (10) and Eq. (21), respectively;
(9) If these values are different from those obtained at step 4, change θ_B and η_B and go back to step 4;
(10) When the actions T_B, M_B and N_B are known, a first value of λ can be computed by means of Eq. (22): if $\lambda < 1$, then $\theta_p = 0$ and go to step 11; if $\lambda > 1$, then increase θ_p and go back to step 5; if $\lambda = 1$, then go to step 11;
(11) Compute the actions H_y and H_z [Eqs.(25)-(26)] and the resistances R_y and R_z [Eqs.(27)];
(12) Compute a new value of λ with Eq. (28): if $\lambda > 1$ then increase d and go back to step 5; if $\lambda \le 1$ then compute the value of pullout load P by means of the following equation (**Fig. 3b**):

$$P = N_B \sin(\alpha + \theta_B) + T_B \cos(\alpha + \theta_B) \tag{29}$$

By repeating this procedure for all the possible values of w, the whole P-w diagram can be evaluated.

4. Validation of the proposed approach

To validate the effectiveness of the proposed cohesive interface model, pullout diagrams are compared with those experimentally measured for different inclination angles α. The tests performed by Leung and Shapiro (1999) on inclined fibers of different yield strengths is here taken into consideration. **Fig. 6a** shows the specimens tested by the Authors. It consists of two blocks made of Plexiglas and cement mortar, respectively. Each fiber is initially locked to the Plexiglas block at three possible inclinations ($\alpha = 90°$, $\alpha = 60°$ and $\alpha = 30°$), then the mortar is cast in steel matching mold. During tests, the diagrams load P vs. displacement w (that is the distance between the two blocks) have been measured (**Fig. 6b**).

From a total of five specimen groups tested by Leung and Shapiro (1999), only the four types reported in **Table 1** are here considered. In the same Table, the mechanical and geometrical properties, as well as the bond and friction properties of the specimens are summarized. Since the type of bond slip relationships and the values of friction angles γ are not reported in the original paper, they have to be estimated.

Referring to the fiber type B, **Fig. 7b** shows the comparison between the theoretical and the experimental results. The specimen with aligned fiber ($\alpha = 90°$) permits to set up the bond-slip relationship. In particular, by assuming the $\tau(s)$ behavior of hot rolled bars, the numerical procedure provides a P-w curve that falls within the range experimentally measured (**Fig. 7a**).

Regarding the friction coefficient γ, it can be indirectly measured by comparing the results of the proposed model and those of pullout tests on inclined fibers. In the case of the fiber type B, if $\gamma = 0.25$ is assumed in the proposed model, the pullout responses are correctly predicted when $\alpha = 60°$ (**Fig. 7b**) and $\alpha = 30°$ (**Fig. 7c**).

These interaction properties are kept for other two fiber types reported in Tab. 1. In fact, they permit to reproduce theoretically all the experimental pullout curves for fiber type C (**Fig. 8**) and fiber type D (**Fig. 9**). In other words, for these fibers, in all the inclinations taken into consideration, the proposed interface cohesive model evaluates pullout loads P which are in good agreement with the range of experimental data measured for all possible displacements ($0 < w < l_i$). Regard-

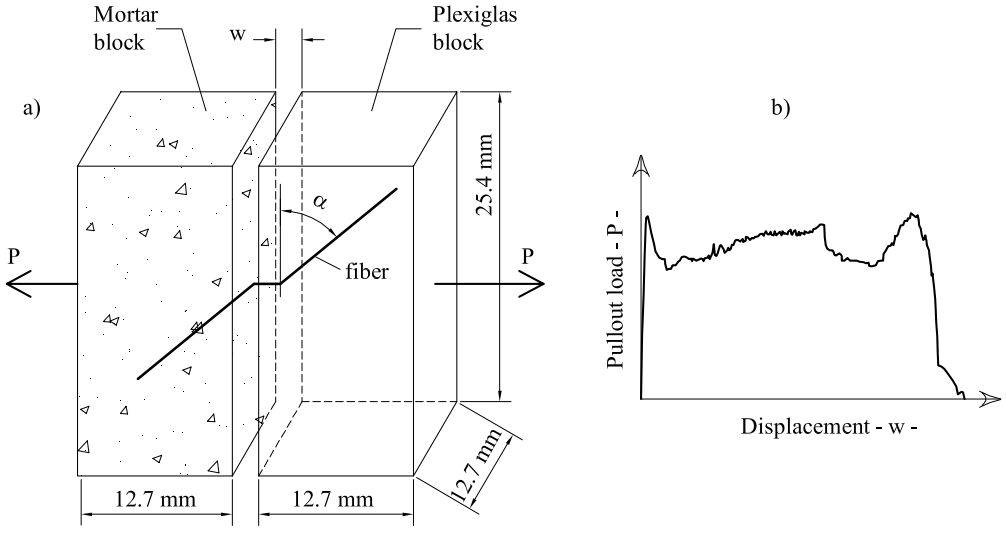

Fig. 6 The pullout tests of Leung and Shapiro (1999): a) geometrical properties of the specimens; b) the curve pullout load P vs. displacement w experimentally measured.

Table 1 mechanical and geometrical properties of the specimens tested by Leung and Shapiro (1999).

	Fiber				Matrix				Interaction (*)	
Type of specimens	Φ (mm)	f_y (MPa)	E_f (GPa)	G_f (GPa)	f_c (MPa)	f_{ct} (MPa)	E_m (GPa)	ν_m	γ	Type of bond
B	0.5	469	200	87	36.5	3.7	30	0.15	0.25	Hot rolled bar
C	0.5	635	200	87	36.5	3.7	30	0.15	0.25	Hot rolled bar
D	0.5	954	200	87	36.5	3.7	30	0.15	0.25	Hot rolled bar
E	0.5	1171	200	87	36.5	3.7	30	0.15	0.15	Cold drawn wires

(*) estimated

ing fiber type E, with a similar procedure, $\tau(s)$ behavior of cold drawn wires and $\gamma = 0.15$ have to be assumed in the proposed model to reproduce the experimental results.

It is important to remark the capability of the proposed model to predict the increase of applied load P before the complete slippage of the fiber, which is clearly evident in all the tests (**Figs.7-9**). Assuming the interaction between fiber and matrix within the block B"-C' (**Fig. 3b**), it is possible to give an explanation to this phenomenon. When the displacement w increases, the length l_{BC} of the embedded fiber becomes progressively shorter. Thus, its mechanical response [Eq.(12)] is that of a short beam [d_{ij} computed with Eq.(15)], which is stiffer than a long beam on elastic foundation [d_{ij} computed with Eq.(16)]. This produces higher shear actions T_B and, despite the decrement of N_B in Eq. (29), the pullout load attains a maximum value just before complete slippage.

Finally, **Fig. 10** shows the maximum values of pullout load at each inclination angle for fiber type D and fiber type E. Both numerical and experimental results reveal a peak of maximum pullout load within the range 954 MPa < f_y <1171 MPa. In fact, the pullout of inclined high strength fibers produces a heavy damage of matrixes having low values of f_c and f_{ct}.

5. Conclusions

A cohesive interface model has been proposed to reproduce theoretically pullout of inclined steel fibers in cement-based matrix. Since a satisfactory agreement between numerical results and experimental data was found, the following conclusions can be drawn:

- To model the action of a fiber that bridges a crack in a fiber reinforced composite, all the nonlinearities and the possible interactions of materials have to be taken into consideration.
- Not only the mechanisms of a beam on elastic foundation have to be introduced in the model, but also the friction coefficient and the bond-slip relationships play a fundamental role in defining the pullout diagram. Since a general definition is not possible, interaction properties should be evaluated for each pair of fiber and matrix.
- Failure criterion and yield surfaces need to be defined in order to reproduce, respectively, the progressive spalling of cementitious matrix and the nonlinear response of steel fibers.

All these aspects (some of them were also measured by previous experimental campaigns) are collected for the first time in the proposed cohesive interface model. The capability of this model to define the complete pullout diagram of inclined fibers, having different yield stresses, seems to have a relevant value, in particular with the aim of designing FRC composites and to optimize their mechanical properties.

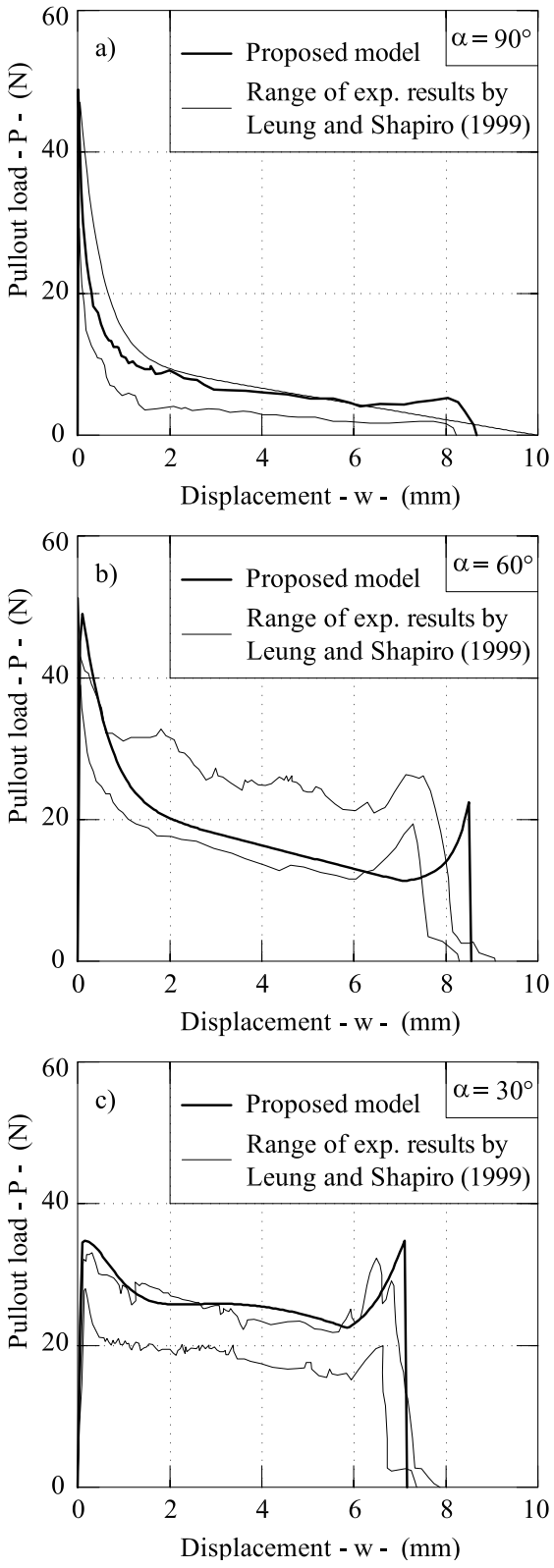

Fig. 7 Comparison between prediction and experimental data for fiber type B; a) pullout load P vs. displacement w in case of $\alpha = 90°$; b) pullout load P vs. displacement w in case of $\alpha = 60°$; c) pullout load P vs. displacement w in case of $\alpha = 30°$.

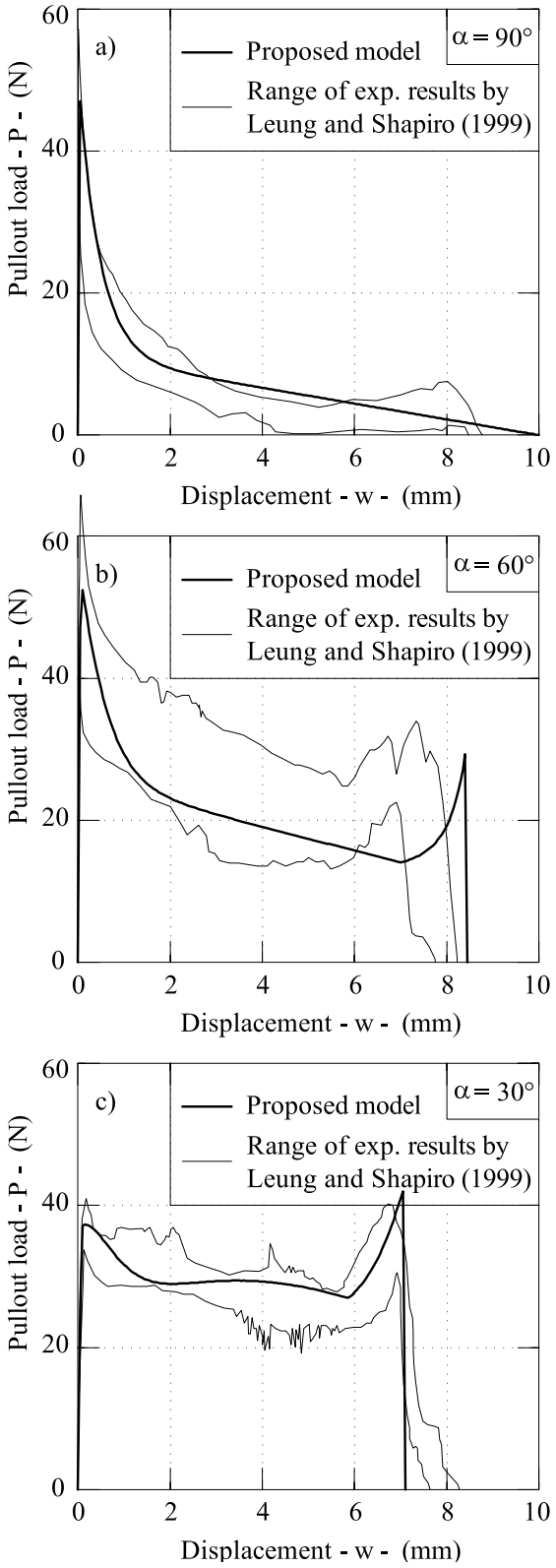

Fig. 8 Comparison between prediction and experimental data for fiber type C; a) pullout load *P* vs. displacement *w* in case of α = 90°; b) pullout load *P* vs. displacement *w* in case of α = 60°; c) pullout load *P* vs. displacement *w* in case of α = 30°.

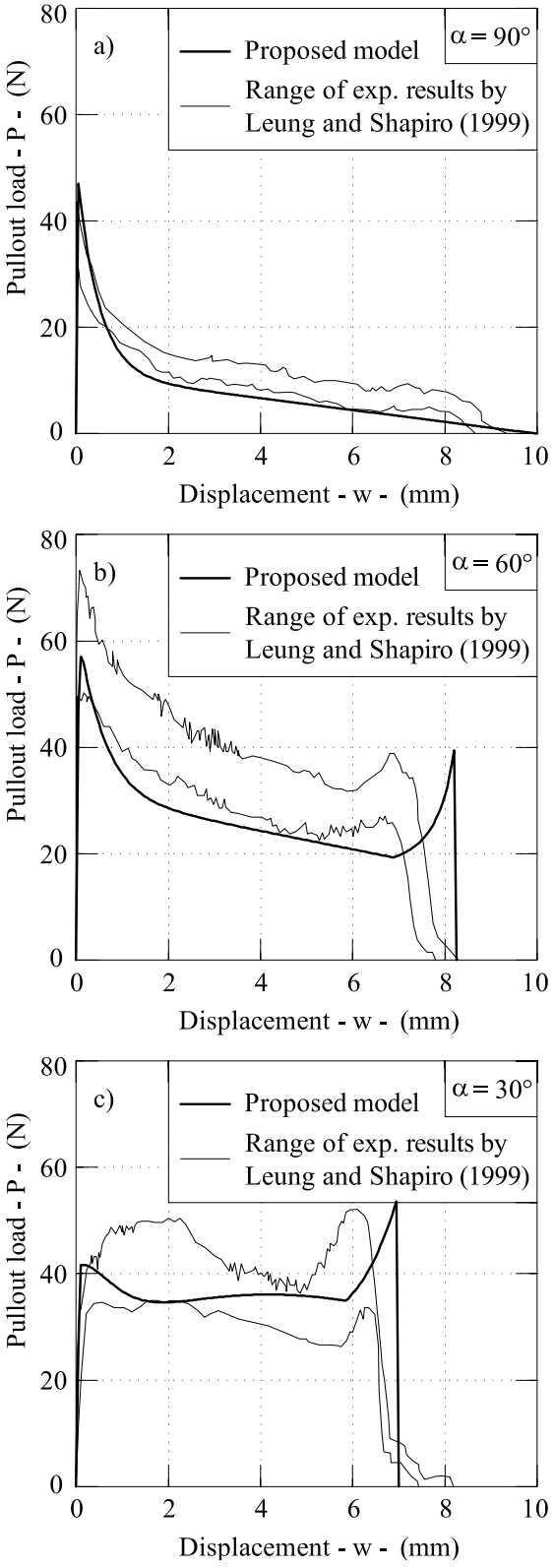

Fig. 9 Comparison between prediction and experimental data for fiber type D; a) pullout load *P* vs. displacement *w* in case of α = 90°; b) pullout load *P* vs. displacement *w* in case of α = 60°; c) pullout load *P* vs. displacement *w* in case of α = 30°.

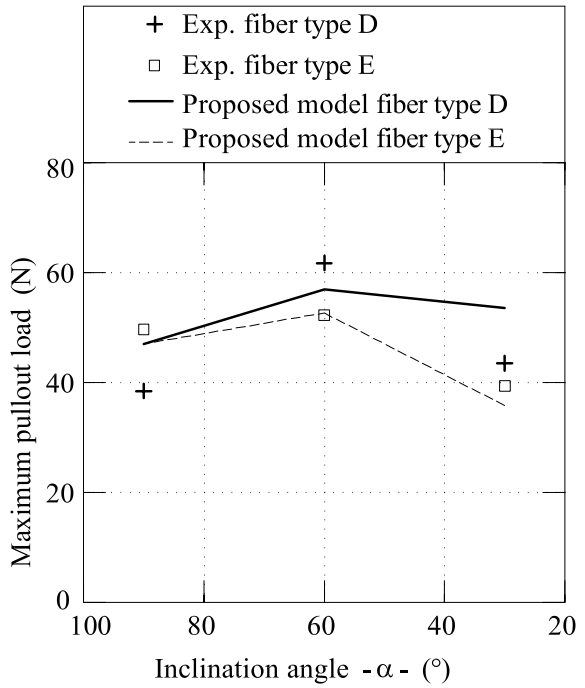

Fig. 10 Maximum pullout load vs. inclination angle for fiber type D and fiber type E.

Acknowledgments

The financial support of Italian Ministry of University and Research (PRIN 2006) is gratefully acknowledged.

Appendix 1: Notations

A_f = Area of the fiber cross-section
E_f = Young's modulus of the fiber
E_m = Young's modulus of the matrix
G_f = Modulus of elasticity in shear
H_y = y component of the loads transferred to the matrix
H_z = z component of the loads transferred to the matrix
J_f = Moment of inertia of the fiber cross-section
K = Matrix foundation stiffness
K_M = Coefficient that computes the component of N_B due to M_B
K_T = Coefficient that computes the component of N_B due to T_B
M = Bending moment in a fiber cross-section
M_0 = Limiting value of bending moment in a fiber cross-section
N = Normal force in a fiber cross-section
N_0 = Limiting values of normal force in a fiber cross-section
N_{bs} = Normal force in a fiber cross-section produced by bond-slip
P = Pullout load
Q = Distributed load on the matrix
R_y = y component of matrix resistance
R_z = z component of matrix resistance
T = Shear force in a fiber cross-section
T_0 = Limiting values of shear force in a fiber cross-section
d = Length of the zone where matrix spalling occurs
d_{ij} = Coefficients of the deformability matrix Eq. (12)
f_c = Compressive strength of the matrix
f_{ct} = Tensile strength of the matrix
f_t = Dimensionless shear constant
f_y = Yield strength of the fiber
k = Coefficient in the bond-slip relationship [Eq. (22b)]
l_{BC} = Length of the embedded part of the fiber (block B"-C')
l_i = Initial length of the fiber
l_0 = Real length of the fiber outside the matrix (block A"-B")
l_t = Apparent length of the fiber outside the matrix (block A"-B")
l_y = Maximum deflection of the fiber (y component of l_0)
l_z = z component of l_0
q_T = Ratio between shear and flexural rotations
s = Slip between fiber and matrix related to point A (**Figs. 1-2**)
s_1 = Slip at τ_{max}
$s_{fm}(\zeta)$ = Function of slips along l_{BC}
w = Displacement of the pullout diagram (half of crack opening displacement)
α = Angle between fiber and crack surfaces
β = Inverse of the characteristic length of the beam on elastic foundation
γ = Friction coefficient between fiber and matrix
δ = Complete rotation of the fiber
Δz = Apparent shortening of the fiber
ε_f = Axial strain of the fiber
Φ = Diameter of the fiber cross-section
η_B = Displacement at point B" (**Fig. 2**)
$\eta_i(z)$ = Function of fiber deflections
λ = Parameters of yield surface of fiber [Eq. (24)] and of failure surface of matrix [Eq. (28)]
ν_m = Poisson's ratio of the matrix
θ_B = Rotation in the point B" (**Fig. 2**)
θ_e = Elastic component of θ_i
θ_i = Rotation produced by bending moment
θ_p = Plastic component of θ_i
θ_t = Rotation produced by shear forces
σ_c = Axial stress of the matrix
σ_f = Axial stress of the fiber
$\tau(s)$ = Bond-slip relationship
τ_{max} = Maximum bond stress
τ_{fin} = Asymptotic value of bond stress
ψ = Angle of principal directions (**Fig. 5b**)
y, z, ζ = Axis of reference systems

Appendix 2: definition of matrix foundation stiffness *K*

Unlike the FEM approach proposed by Leung and Li (1992), the matrix foundation stiffness is here computed by means of a simplified model, which is based on the hypotheses of stress-distribution shown in **Fig. 3c**. Under the conditions of plane strain and linear elastic be-

havior of the matrix (defined by the parameters E_m and ν_m), it is possible to write:

$$\sigma_y(y)=\frac{Q}{\Phi+2y} \quad \text{and} \quad \varepsilon_y(y)=\frac{\sigma_y(y)}{E_m\left(1-\nu_m^2\right)} \tag{A1}$$

where Q = distributed load on the matrix produced by the length l_{BC} of the fiber.

At depth t, the displacement η is equal to:

$$\eta=\int_0^t \varepsilon_y(y)\,dy=\frac{P}{E_m\left(1-\nu_m^2\right)}\int_0^t \frac{dy}{\Phi\left(1+2\,y/\Phi\right)} = \frac{Q}{2E_m\left(1-\nu_m^2\right)} ln\left(1+2\frac{t}{\Phi}\right) \tag{A2}$$

Thus, the matrix foundation stiffness is:

$$K=\frac{Q}{\eta}=\frac{E_m\left(1-\nu_m^2\right)}{0.5\ln\left(1+2\frac{t}{\Phi}\right)} \tag{A3}$$

To obtain K, it is necessary to introduce a suitable value of t, which is the thickness of the matrix around the fiber. Since the presence of nonlinearities implies reduced values of matrix foundation stiffness, like in the case of high values of t, K is here defined by assuming $t = 100\ \Phi$. In this case Eq. (A3) gives:

$$K=\frac{Q}{\eta}=\frac{E_m\left(1-\nu_m^2\right)}{2.651} \tag{A4}$$

References

Bazant, Z. P., Li, Z. and Thoma, M. (1995). "Identification of stress-slip law for bar or fiber pullout by size effect tests." *ASCE Journal of Engineering Mechanics*, 121(5), 620-625.

Bowles, J. E. (1988). "*Foundation analysis and design.*" 4th edition, New York: McGraw-Hill.

Brandt, A. M. (1985). "On the optimal direction of short metal fibres in brittle matrix composites." *Journal of Materials Science*, 20, 3831-3841.

CEB-FIP, (1991). "*CEB-FIP Model Code 1990.*" Bulletin d'information 203-205. London: Thomas Telford.

Chen, W. F. and Han, D. J. (1988). "*Plasticity for structural engineers.*" New York: Springer.

Fantilli, A. P., Ferretti, D., Iori, I. and Vallini, P. (1998). "Flexural Deformability of Reinforced Concrete Beams." *ASCE Journal of Structural Engineering*, 124(9), 1041-1049.

Fantilli, A. P. and Vallini, P. (2003a). "A cohesive model for fiber-reinforced composites." *In*: F. Bontempi Ed. *ISEC-02 Second International Structural Engineering and Construction Conference*, Rome, *23-26 September 2003*. Lisse: A. A. Balkema Publishers, 1443-1449.

Fantilli, A. P. and Vallini, P. (2003b). "Bond-slip relationship for smooth steel reinforcement." *In:* N. Bicanic, R. de Borst, H. Mang and G. Meschke, Eds. *Computational Modelling of Concrete Structures (EURO-C 2003)*, St. Johann Im Pongau *17-20 March 2003*. Lisse: A.A. Balkema Publishers, 215-224.

Hetenyi, M. (1946). "*Beams on elastic foundation.*" Ann Arbor: The University of Michigan Press.

Hillerborg, A. (1980). "Analysis of fracture by means of the fictitious crack model, particularly for fibre reinforced concrete." *The International Journal of Cement Composites*, 2(4), 177- 184.

Katz, A. and Li, V. C. (1995). "Inclination angle effect of carbon fibers in cementitious composites." *ASCE Journal of Engineering Mechanics*, 121(12), 1340-1348.

Kohno, Y. and Mihashi, H. (2005). "Basic research on the mechanism of enhancing toughness on fiber reinforced cementitious composites." *Cement Science and Concrete Technology*, 59, 404-410. (In Japanese)

Leung, C. K. Y. and Li, V. C. (1992). "Effect of fiber inclination on crack bridging stress in brittle fiber reinforced brittle matrix composites." *Journal of the Mechanics and Physics of Solids*, 40(6), 1333-1362.

Leung, C. K. Y. and Shapiro, N. (1999). "Optimal steel fiber strength for reinforcement of cementitious materials." *ASCE Journal of Materials in Civil Engineering*, 11(2), 116-123.

Morton, J. and Groves, G. W. (1974). "The cracking of composites consisting of discontinuous ductile fibres in a brittle matrix – effect of fibre orientation." *Journal of Materials Science*, 9, 1436-1445.

Naaman, A. E. and Shah, S. P. (1976). "Pull-out mechanism in steel fiber-reinforced concrete." *ASCE Journal of the Structural Division*, 102(8), 1537-1548.

Shah, S. P., Kuder, K. G. and Mu, B. (2004). "Fiber-reinforced cement-based composites: a forty year odyssey." *In:* M. di Prisco, R. Felicetti and G. A. Plizzari, Eds. Fibre-Reinforced Concretes (BEFIB 2004), Varenna *20-22 September 2004*. Bagneux: Rilem Publications S.A.R.L., 3-30.

Shah, S. P. and Ouyang, C. (1991). "Mechanical behavior of fiber-reinforced cement-based composites." *Journal of the American Ceramic Society*, 74(11), 2727-38, 2947-53.

Stang, H., Li, Z. and Shah, S. P. (1990). "Pullout problem: Stress versus fracture mechanical approach." *ASCE Journal of Engineering Mechanics*, 116(10), 2136-2150.